Eurasia Specialized Veterinary Publication

International Journal of Veterinary Research and Allied Science

ISSN:3062-357X

2023, Volume 3, Issue 2, Page No: 79-93

Available online at: www.esvpub.com/

Synergistic Cardiac Repair Post-Myocardial Infarction Using Adipose-Derived Stem Cell-Seeded Decellularized Porcine Pericardium: Functional and Histological Evidence

Mariam Adel[1], Youssef Ibrahim[1*], Yasmin Hassan[1]

[1]Department of Veterinary Surgery, Faculty of Veterinary Medicine, Suez Canal University, Ismailia 41522, Ismailia, Egypt.

***E-mail** ✉ youssefibrahim88@gmail.com

ABSTRACT

Myocardial infarction (MI) remains one of the most critical cardiovascular disorders and continues to be the foremost global cause of mortality. Therefore, regenerating damaged cardiac tissue is a key focus in restoring cardiac performance after MI. This study explored the potential of rat adipose-derived mesenchymal stem cells (r-AdMSCs) combined with decellularized porcine pericardium (DPP) to repair myocardial function in MI-induced rats. MI was produced in four experimental groups: one untreated and three treated with either DPP alone (MI-DPP), stem cells alone (MI-SC), or both (MI-SC/DPP). Cardiac function in all groups, including the Sham group, was assessed via echocardiography and intraventricular pressure gradient (IVPG) at weeks 2 and 4, alongside hemodynamic testing in week 4. On day 31, all animals were euthanized for histopathological evaluation. The echocardiographic, IVPG, and hemodynamic data confirmed that all treatments aided cardiac recovery, though the MI-SC/DPP group exhibited significantly greater functional improvement compared to the other interventions. Histological results revealed that this group had the lowest ($p < 0.05$) levels of degeneration and fibrosis among all treated sets. Overall, DPP scaffolds seeded with stem cells offer a highly effective platform for stem cell delivery and cardiac regeneration post-MI.

Keywords: Adipose stem cells, Decellularized porcine pericardium, DPP, Biomaterials, Tissue regeneration, Cell delivery

Received: 22 August 2023
Revised: 24 November 2023
Accepted: 26 November 2023

How to Cite This Article: Adel M, Ibrahim Y, Hassan Y. Synergistic Cardiac Repair Post-Myocardial Infarction Using Adipose-Derived Stem Cell-Seeded Decellularized Porcine Pericardium: Functional and Histological Evidence. Int J Vet Res Allied Sci. 2023;3(2):79-93. https://doi.org/10.51847/mSI4sIeJh3

Introduction

Cardiovascular diseases are recognized as the primary cause of global mortality [1]. Among them, myocardial infarction (MI) is a major condition leading to severe cardiac dysfunction, frequently resulting in heart failure or death. Despite advancements in medical and surgical management, MI can still lead to complications such as ischemic cardiomyopathy [2]. Recently, cardiac tissue regeneration has emerged as a promising approach for restoring heart function following MI [3, 4]. Adipose-derived mesenchymal stem cells (AdMSCs) have demonstrated notable potential in this field, promoting neovascularization of damaged myocardium through the release of multiple growth factors, including basic fibroblast growth factor (bFGF), vascular endothelial growth factor (VEGF), and hepatocyte growth factor (HGF) [5, 6]. Moreover, they contribute to enhanced cardiac remodeling and contractility, supporting functional recovery [7, 8]. Over time, numerous studies have sought to improve AdMSC-based therapies through methods such as genetic modification to enhance survival and homing efficiency [9, 10].

Tissue engineering has also become a rapidly growing field, utilizing innovative biomaterials and technologies to support organ and tissue repair [11]. Various natural and synthetic scaffolds have been investigated for cardiac tissue engineering (CTE) [12–18]. Although synthetic scaffolds provide structural reinforcement and influence tissue remodeling, they often fall short due to limited regenerative capability, inability to integrate with native tissues, and lack of contractility [19, 20]. Consequently, natural decellularized extracellular matrix (ECM) materials derived from sources such as the pericardium [21–23], urinary bladder [24], stomach [25], small intestine [26], and amniotic membrane [27] have gained considerable interest as superior alternatives for CTE [28]. ECM components furnish a biologically favorable microenvironment that facilitates the retention and functionality of transplanted stem cells at the infarct site [29, 30].

Although autologous biomaterials have been applied in several animal studies, their limited availability poses practical constraints. Hence, xenograft-derived ECM scaffolds have been developed as a viable solution due to their lower immunogenicity and enhanced potential for recellularization, supporting cellular adhesion, migration, and proliferation [31–33]. Seeding decellularized scaffolds with mesenchymal stem cells (MSCs) has further improved outcomes by promoting integration and tissue remodeling [34]. Notably, MSCs express minimal levels of MHC class I and II molecules, reducing immunological rejection [35]. Embedding these cells within a natural scaffold is more beneficial than direct injection, as it mitigates the harsh post-MI environment and enhances cell survival and retention [36, 37].

Functional recovery of these engineered constructs is often assessed using imaging techniques. Echocardiography remains the standard, offering a non-invasive and radiation-free modality suitable for longitudinal monitoring [38]. Recently, intraventricular pressure gradient (IVPG) imaging has emerged as a sensitive echocardiographic parameter capable of detecting functional changes earlier than conventional methods by quantifying intraventricular flow and pressure alterations [39–41]. To our knowledge, this represents the first study to employ IVPG assessment following combined cell- and biomaterial-based cardiac therapies. Thus, this research aims to evaluate the regenerative potential of decellularized porcine pericardium (DPP) seeded with r-AdMSCs for cardiac tissue repair and to determine the value of IVPG in assessing cardiac function recovery.

Materials and Methods

Experimental animals

A total of thirty male Sprague Dawley (SD) rats (Kitayama Labes Co., Ltd., Nagano, Japan) aged three months and weighing 376.30 ± 27.24 g were enrolled. The rats were maintained individually in cages at 25 ± 2 °C under a 12-hour light/dark cycle, with free access to food and water. All animal handling and experimental work were approved by the Institutional Animal Care and Use Committee of the Tokyo University of Agriculture and Technology (approval code: R05-91) and conducted in compliance with the NIH Guide for the Care and Use of Laboratory Animals.

Study layout

Animals were separated into five groups (n = 6 each). Myocardial infarction (MI) was experimentally produced in four groups, while three of those received specific interventions.

- Sham group: thoracotomy performed, but MI not induced.
- MI group: MI surgically induced, no further treatment.
- MI-DPP group: MI followed by implantation of decellularized porcine pericardium (DPP).
- MI-SC group: MI treated by injection of rat adipose-derived mesenchymal stem cells (r-AdMSCs).
- MI-SC/DPP group: MI treated with stem-cell-seeded DPP.

Cardiac function was analyzed by transthoracic echocardiography and color M-mode echocardiography (CMME) to evaluate the intraventricular pressure gradient (IVPG) at weeks 2 and 4 post-surgery. On day 91, hemodynamic data (intraventricular pressure indices) were recorded under 1.5–2% isoflurane anesthesia **(Figure 1)**. Finally, animals were euthanized with excess isoflurane, and hearts were collected for histopathological study.

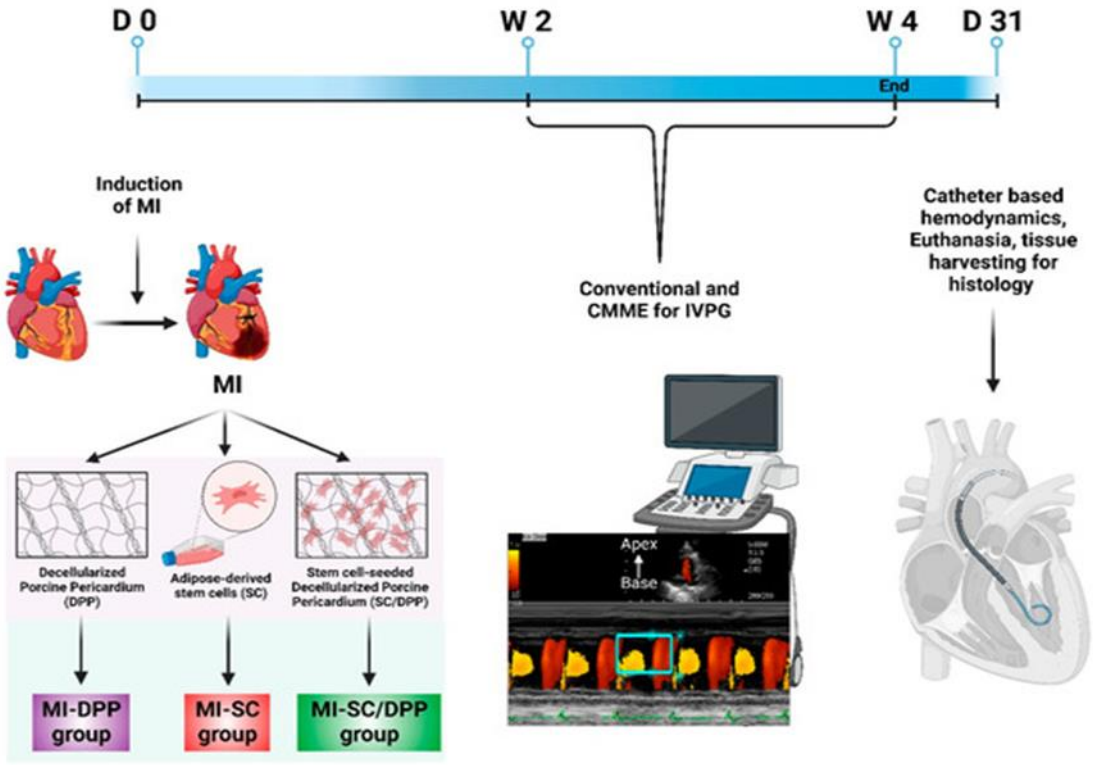

Figure 1. Diagram summarizing the experimental workflow.

Isolation and identification of r-AdMSCs

Adipose tissue was obtained from the inguinal area of five healthy SD rats (2 months old; 250–300 g) under sterile conditions. r-AdMSCs were isolated as outlined in a previously established method [5]. In summary, the excised fat was rinsed with PBS, minced finely, and digested with 0.1% (w/v) collagenase type I (1 mg/mL; Gibco, Life Technologies, Waltham, MA, USA) at 37 °C for one h. The digest was then centrifuged (800×g for 10 min), filtered through 100 µm strainers, and treated for RBC lysis. Cell pellets were resuspended in Dulbecco's Modified Eagle Medium (DMEM; 043-30085, Fujifilm Wako Pure Chemical Corp., Osaka, Japan).

Cells were plated (5×10^5 cells per 75 cm^2 dish) in DMEM + 10% fetal bovine serum (FBS) and cultured at 37 °C, 5% CO_2, and 95% humidity. The medium was renewed every three days until reaching 80% confluence, then sub-cultured. Passage 3 (P3) cells were employed for in vivo use. Morphological, immunophenotypic (flow cytometry), and tri-lineage (adipogenic, osteogenic, chondrogenic) differentiation profiles were verified as reported previously [5].

Preparation and evaluation of DPP scaffold

Decellularized porcine pericardium (DPP) scaffolds were produced according to an adjusted version of our earlier method [6], based on Ramm *et al*., 2020 [42]. Fresh pericardial tissues were collected from healthy 5–6-month-old pigs (both sexes) obtained from a Tokyo slaughterhouse. Samples were trimmed to remove fat and connective tissue, washed with PBS, and disinfected with sodium Braunol® (B. Braun) under shaking for 5 min.

Decellularization proceeded through sequential incubations:

1. Trypsin 0.125% + EDTA 0.05% (T4049-100 ML, Sigma Aldrich, St. Louis, MO, USA) for 90 min,
2. Triton X-100 (0.5%) for two 12-h cycles,
3. Sodium dodecyl sulfate (SDS 0.5%, L3771, Sigma Aldrich) for two 12-h cycles, followed by two water washes (12 h each) and 14 PBS rinses (12 h each).

The decellularized tissues were preserved in PBS + antibiotics (penicillin, streptomycin, and amphotericin B each 1 mg/mL) at 4 °C until use. All incubations were performed on an orbital shaker (200 rpm) at room temperature. Microstructural, mechanical, and biocompatibility analyses of these DPP matrices were described comprehensively in our prior publication [6].

Construction of stem-cell-seeded DPP

Sterile DPP membranes were cut into 1.5 × 1.5 cm^2 segments and pre-incubated for 24 h in DMEM within culture plates. Following this, r-AdMSCs were seeded using the protocol of previous studies [21, 43]. In short, 1.0 × 10^6 cells were suspended in 50 µL culture medium and evenly dispensed onto each DPP piece, allowing 30 h of adherence. Additional medium drops were then applied, followed by another 90-minute incubation. Finally, 20 mL of DMEM was added to each plate. The cell-seeded DPP scaffolds were maintained at 37 °C, 5% CO_2, and 95% humidity for 5–7 days before implantation.

Induction and treatment of myocardial infarction

MI was generated following established techniques [44]. Under anesthesia, rats were intubated and ventilated using a rodent ventilator (Harvard Apparatus, Boston, MA, USA) delivering a 1.5–2% isoflurane-oxygen mixture. A left-sided thoracotomy was made at the fourth intercostal space, exposing the left anterior descending (LAD) artery, which was tied 4–5 mm below the atrioventricular junction with 6-0 Prolene suture. Blanching of the left ventricle distal to the ligation confirmed infarction.

Immediately after MI induction, animals received treatments depending on group assignment [45, 46].

- MI-DPP group: DPP patch placed directly over the infarct region.
- MI-SC group: injection of 100 µL r-AdMSCs suspension (1.0 × 10^6 cells/rat) at multiple points within and around the infarct area.
- MI-SC/DPP group: implantation of stem-cell-seeded DPP over the infarcted myocardium.

Cardiac function assessment

To evaluate the restorative potential of the stem cell–seeded DPP on cardiac performance following myocardial infarction (MI), we applied standard echocardiography, CMME-based IVPG measurement, and catheter-derived hemodynamic analysis **(Figure 1)**.

Standard echocardiography

Echocardiographic imaging was performed in accordance with the American Society of Echocardiography (ASE) recommendations [47] and the procedures described by Zacchigna *et al*. [48]. All recordings were obtained using a ProSound 7 ultrasound unit (Hitachi-Aloka Medical Ltd., Tokyo, Japan) fitted with a 12 MHz transducer, equipped for CMME and synchronized with ECG monitoring. The methodology and analytical approach followed those reported in our earlier publications [40].

Intraventricular pressure gradient (IVPG)

The CMME modality was employed to determine IVPG as previously described in detail in our prior work. Imaging parameters included a sweep speed of 300 mm/s and a color baseline offset of −64, optimizing the Nyquist limit for accurate CMME tracing. Captured CMME frames were processed using MATLAB software (The MathWorks, Natick, MA, USA) to generate both spatial and temporal IVPG profiles. Measurements were extracted from four segments of the left ventricle (LV): basal, mid, mid-to-apical (MA), and apical regions. The total IVPG was calculated as the sum of all segmental gradients.

Catheter-based hemodynamic analysis

On day 31, under inhalational anesthesia, a 2-Fr microtip pressure catheter (SPR-407, Mikro-Cath, Millar Instruments, Houston, TX, USA) was introduced retrogradely via the right carotid artery into the LV cavity to record intraventricular pressures and related hemodynamic parameters. To minimize respiration-induced fluctuations, ventilation was briefly paused during data collection. Each measurement set covered 10–15 consecutive cardiac cycles, and averaged values were used for subsequent analysis. Hemodynamic data were processed using LabChart Pro software (version 8, AD Instruments, Colorado Springs, CO, USA), consistent with prior analytical protocols [40].

Histological examination

After euthanasia, excised cardiac tissues from all groups were rinsed in PBS, fixed in 4% buffered formalin, embedded in paraffin, and sectioned into five µm slices. Sections underwent xylene deparaffinization, followed

by graded ethanol dehydration, and were stained with hematoxylin and eosin (H&E) to evaluate cardiac architecture.

For regeneration analysis, ten H&E-stained slides per group were assessed by a blinded histopathologist for parameters including mononuclear cell infiltration, fibrotic or necrotic regions, interstitial edema, and organization of cardiomyocytes. The severity of histopathological alterations was scored following the criteria in [49]: 0 = no changes, 1 = mild, 2 = moderate, 3 = severe, and 4 = very severe.

The extent of fibrosis was quantified using Masson's trichrome (MTC) staining. The fibrotic area (%) was determined with NIH ImageJ software as: (Fibrosis % = (fibrosis area/LV wall area) × 100) following the procedure outlined in [46].

Statistical analysis

Results were expressed as mean ± standard deviation (SD). Differences in echocardiographic and IVPG values among groups at weeks 2 and 4 were analyzed via two-way ANOVA with Tukey's post hoc test. Meanwhile, hemodynamic parameters, histopathological scores, and fibrotic area percentages obtained at the study's conclusion were compared using the Kruskal–Wallis one-way ANOVA followed by Dunn's post hoc test. All statistical processing was carried out using GraphPad Prism 9 (GraphPad Software, Inc., La Jolla, CA, USA). A p-value < 0.05 was considered to indicate statistical significance.

Results and Discussion

In this investigation, both decellularized porcine pericardium (DPP) and adipose-derived stem cells (AdMSCs) demonstrated considerable potential to enhance cardiac recovery following MI. However, when used together as a combined therapy, the DPP–stem cell construct exhibited a notably synergistic effect, producing the most pronounced improvement in cardiac function. This conclusion was consistently supported across multiple evaluation methods, including echocardiographic imaging, IVPG mapping, hemodynamic testing, and histological assessments.

Echocardiography

Modifications in echocardiographic parameters among experimental groups are summarized in **Table 1** and **Figures 2 and 3**. Analysis of cardiac imaging demonstrated that both decellularized biomaterial (MI-DPP) and adipose-derived stem cells (MI-SC) provided partial functional recovery of the myocardium and mitigated the deterioration caused by MI. In contrast, animals receiving stem cell–incorporated DPP (MI-SC/DPP) exhibited the most pronounced reparative outcomes, showing superior recovery and maintenance of cardiac performance. Furthermore, this effect became more apparent as time progressed.

No major difference was noted between MI-DPP and MI-SC groups, except that the MI-DPP animals displayed a greater LV internal diameter at systole (LVIDs) and a lower fractional shortening (FS) during week 2 (W2) compared to MI-SC **(Table 1)**. By week 4 (W4), significant reductions were detected in LV internal diameter at diastole (LVIDd), LVIDs, posterior wall thickness at diastole (LVPWd), posterior wall thickness at systole (LVPWs), and LV mass (LVM) in the MI-SC/DPP rats compared with both the MI ($p < 0.0001$) and MI-DPP ($p < 0.01$) groups. Comparable tendencies appeared at W2, although LVPWd and LVM did not differ significantly. Indices such as septal thickness at diastole (IVSd), septal thickness at systole (IVSs), ejection fraction (EF), and fractional shortening (FS) were markedly elevated in the MI-SC/DPP animals at W4 relative to MI and MI-DPP. Similar trends were observed at W2, with the exception that IVSs were not significantly altered.

As depicted in **Figures 2 and 3**, evaluation of diastolic properties through Tissue Doppler Imaging (TDI) revealed substantial differences among the groups. Both systolic (s′) and early diastolic (e′) myocardial wall velocities, as well as the e′/a′ ratio, increased considerably in all treated animals relative to MI controls. Conversely, the late diastolic wall velocity (a′), on both the septal and lateral walls, was reduced in the MI-DPP, MI-SC, and MI-SC/DPP cohorts compared with the MI group throughout the study period **(Figure 2)**.

In terms of transmitral flow, a clear decrease in early diastolic flow velocity (E) and the E/A ratio was identified in the MI-SC/DPP group compared with MI and MI-DPP during W2 and W4, whereas the late diastolic (A) wave was increased. There were no significant differences between MI-SC and MI-SC/DPP in these flow indices. Moreover, the E/septal e′, E/lateral e′, and E/e′ ratios were consistently lower in treated groups relative to MI controls **(Figure 3)**.

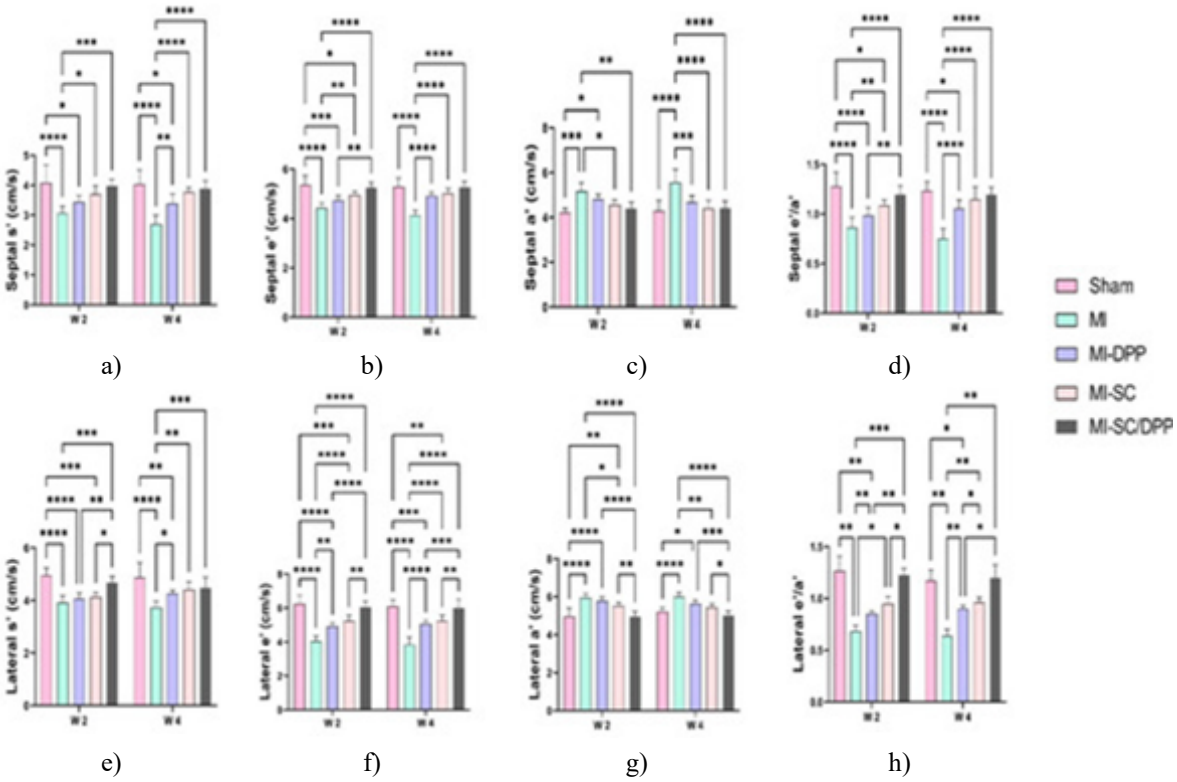

a) b) c) d)

e) f) g) h)

Figure 2. Tissue Doppler Imaging (TDI) demonstrating the restorative influence of the stem cell–loaded scaffold on diastolic function after myocardial infarction. Data expressed as mean ± SD. * $p < 0.05$, ** $p < 0.01$, *** $p < 0.001$, **** $p < 0.0001$.

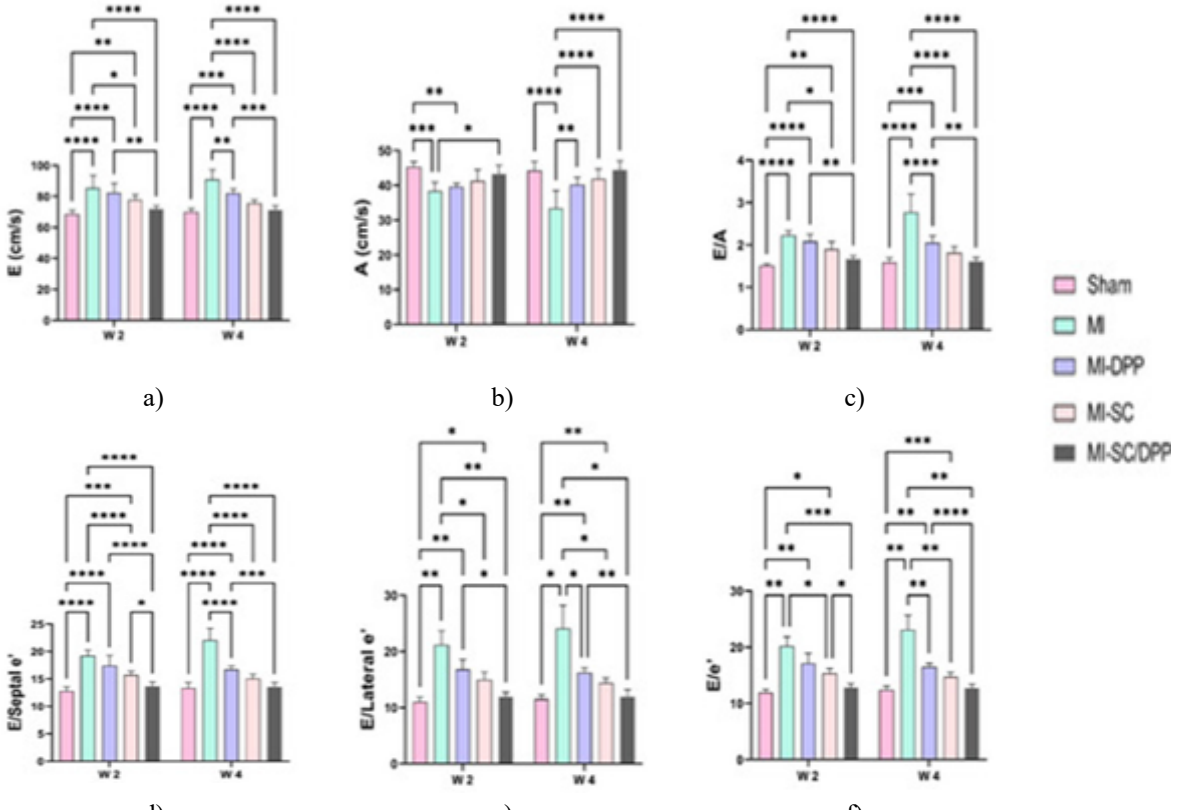

a) b) c)

d) e) f)

Figure 3. Transmitral flow echocardiography illustrating the effectiveness of the stem cell–infused DPP in improving diastolic capacity following MI. Data are shown as mean ± SD. * $p < 0.05$, ** $p < 0.01$, *** $p < 0.001$, **** $p < 0.0001$.

Table 1. Echocardiographic cardiac function parameters across experimental groups.

					Time					
Parameters	**Sham**	**MI**	**MI-DPP**	**MI-SC**	**MI-SC/DPP**	**Sham**	**MI**	**MI-DPP**	**MI-SC**	**MI-SC/DPP**
					W 2					**W 4**
Dimensional indices										
LVIDd (mm)	6.45 ± 0.43	7.83 ± 0.41 ****	7.37 ± 0.20 ***	6.88 ± 0.24 ††††	6.67 ± 0.17 ††††‡‡	6.40 ± 0.34	8.88 ± 0.41 ****	7.15 ± 0.17 **†††††	6.68 ± 0.24 ††††	6.23 ± 0.20 ††††‡‡‡
IVSd (mm)	2.07 ± 0.26	1.52 ± 0.20 ****	1.63 ± 0.17 **	1.73 ± 0.15 *	1.97 ± 0.11 †††‡	2.10 ± 0.26	1.50 ± 0.13 ****	1.73 ± 0.15 *	1.90 ± 0.08 ††	1.97 ± 0.11 †††
LVPWd (mm)	1.70 ± 0.21	1.90 ± 0.31	1.88 ± 0.13	1.77 ± 0.11	1.68 ± 0.11	1.75 ± 0.10	2.13 ± 0.29 *	1.80 ± 0.13 †	1.68 ± 0.20 ††	1.63 ± 0.11 †††
LVIDs (mm)	3.60 ± 0.22	5.15 ± 0.28 ****	4.53 ± 0.15 ****††	3.98 ± 0.21 †††††‡	3.80 ± 0.16 ††††‡‡‡	3.70 ± 0.26	6.70 ± 0.49 ****	4.30 ± 0.13 **†††††	3.97 ± 0.20 ††††	3.78 ± 0.29 †††††‡
IVSs (mm)	2.02 ± 0.11	1.70 ± 0.21 *	1.72 ± 0.14 *	1.82 ± 0.26	1.95 ± 0.10	2.07 ± 0.20	1.47 ± 0.14 ****	1.73 ± 0.07 **	1.78 ± 0.11 *†	1.93 ± 0.07 †††
LVPWs (mm)	2.48 ± 0.16	1.95 ± 0.17 ****	1.95 ± 0.19 ****	2.10 ± 0.08 **	2.15 ± 0.13 *	2.27 ± 0.17	1.60 ± 0.24 ****	1.92 ± 0.23 *†	2.15 ± 0.10 ††††	2.08 ± 0.11 †††
LVM (mg)	667.9 ± 117.47	787.52 ± 123.24	741.62 ± 65.57	660.78 ± 46.03	668.71 ± 58.52	678.45 ± 63.15	1052.83 ± 134.25 ****	711.89 ± 55.78 ††††	652.32 ± 51.27 ††††	590.92 ± 54.69 ††††
Functional parameters										
EF (%)	86.73 ± 1.79	57.6 ± 2.88 ****	60.7 ± 1.33 ****	66.05 ± 3.83 ****†† ††‡	76.1 ± 2.34 ****†† ††‡‡‡‡ ####	84.82 ± 2.22	54.48 ± 5.09 ****	65.97 ± 2.74 ****†† ††	72.67 ± 2.11 ****†† ††‡‡	80.32 ± 1.30 ††††‡‡ ‡‡##
FS (%)	48.53 ± 1.74	32.73 ± 4.01 ****	33.05 ± 2.69 ****	38.03 ± 2.81 ****†‡	42.48 ± 2.23 **†††† ‡‡‡‡	46.68 ± 2.59	31.23 ± 1.05 ****	35.53 ± 2.29 ****	37.95 ± 2.66 ****††	43.55 ± 2.71 ††††‡‡ ‡‡#

Results are presented as mean ± SD. * $p < 0.05$, ** $p < 0.01$, *** $p < 0.001$, **** $p < 0.0001$ vs. Sham; † $p < 0.05$, †† $p < 0.01$, ††† $p < 0.001$, †††† $p < 0.0001$ vs. MI; ‡ $p < 0.05$, ‡‡ $p < 0.01$, ‡‡‡ $p < 0.001$, ‡‡‡‡ $p < 0.0001$ vs. MI-DPP; # $p < 0.05$, ## $p < 0.01$, #### $p < 0.0001$ vs. MI-SC.

Intraventricular pressure gradient (IVPG)

The contribution of the stem cell–biomaterial complex to cardiac functional recovery, analyzed through CMME-derived IVPG, is represented in **Figure 4**. Variations were evident in both overall and regional IVPG profiles. Treated animals exhibited elevated total, mid, mid-apical (MA), and apical IVPG values when compared with the MI group, while the basal IVPG was consistently lower.

In terms of total IVPG, MI-SC/DPP rats displayed significantly higher values than MI animals at W2, and higher than both MI and MI-DPP groups by W4. There was no noteworthy variation in total IVPG between MI-SC and MI-SC/DPP throughout the study.

For segmental measurements, the basal IVPG was substantially reduced in the MI-SC/DPP group relative to MI, MI-DPP, and MI-SC. Similarly, both MI-DPP and MI-SC groups showed lower basal IVPG compared with MI

at W2 and W4. The mid-IVPG increased notably ($p < 0.05$) in the MI-SC/DPP group compared with MI and MI-DPP at both intervals ($p < 0.05$, $p < 0.0001$, respectively). No difference appeared between MI-SC and MI-SC/DPP at W2, but a significant rise ($p < 0.05$) occurred at W4.

The MA IVPG was also considerably higher in MI-SC/DPP compared to MI and MI-DPP, with MI-SC showing intermediate but significant improvement versus MI throughout. No distinction was noted between MI-SC and MI-SC/DPP for this parameter. The apical IVPG rose sharply in the MI-SC/DPP group compared to MI and MI-DPP at both W2 and W4, while remaining comparable to MI-SC. Additionally, the MI-SC animals showed an increased apical IVPG ($p < 0.01$) relative to MI controls **(Figure 4)**.

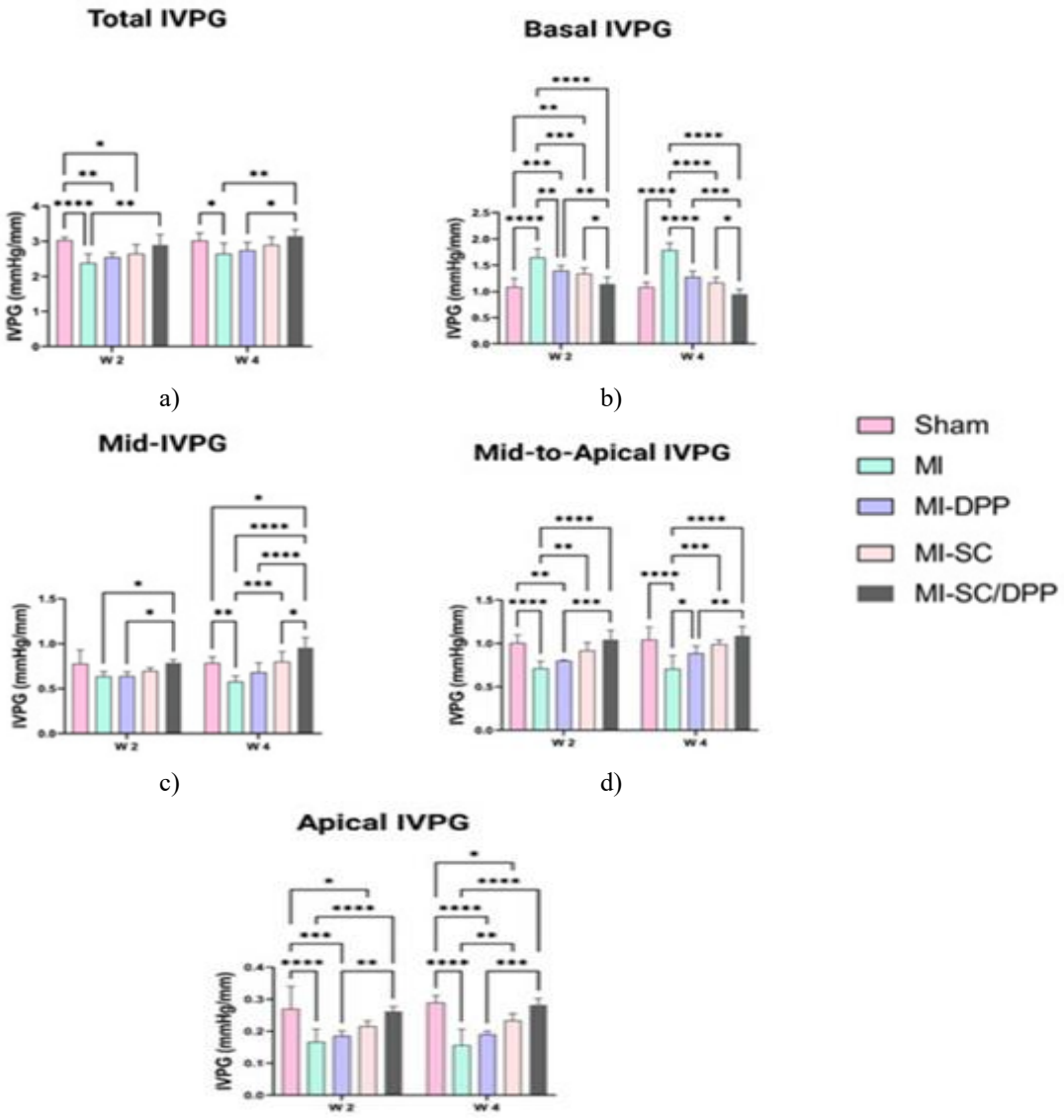

Figure 4. Intraventricular pressure gradient (IVPG) illustrating the restorative potential of stem cell–integrated biomaterial on diastolic performance after myocardial infarction (MI). Results expressed as mean ± SD. *$p < 0.05$, ** $p < 0.01$, *** $p < 0.001$, **** $p < 0.0001$.

Intra-ventricular catheter-derived hemodynamic evaluation

The end-point comparisons of ventricular pressure-based parameters across experimental groups are summarized in **Figure 5**. The systolic blood pressure (SBP) values were highest in the MI-SC/DPP animals, exceeding those recorded in the MI, MI-DPP, and MI-SC groups. Conversely, the MI group exhibited significantly lower SBP when compared with sham, MI-DPP, and MI-SC subjects. The difference between MI-DPP and MI-SC was not statistically notable.

Both the maximum rate of LV pressure rise (dP/dtmax) and the maximum rate of pressure decline (−dP/dtmin)

showed pronounced increases in MI-SC/DPP relative to MI. Additionally, −dP/dtmin was significantly higher in MI-SC/DPP compared with MI-DPP ($p < 0.05$). No marked variation was found between MI-SC and MI-SC/DPP groups for either +dP/dt or −dP/dt values.

The left ventricular end-diastolic pressure (LVEDP) was greatly elevated in MI animals compared with the sham, MI-DPP, MI-SC, and MI-SC/DPP groups ($p < 0.0001$, $p < 0.05$, $p < 0.01$, and $p < 0.0001$, respectively). In contrast, MI-SC/DPP animals displayed notably reduced LVEDP compared with both MI-DPP and MI-SC.

Similarly, the isovolumic relaxation time constant (Tau, τ) was significantly shorter in MI-SC/DPP animals relative to MI-SC and MI. Distinct differences were also noted between MI-SC and MI-DPP for both LVEDP and Tau indices.

A clear increase in heart rate (HR) was recorded in MI animals when compared to all treated groups. Although MI-DPP, MI-SC, and MI-SC/DPP showed no meaningful variation among themselves, HR in MI-DPP and MI-SC remained considerably above that in the sham controls **(Figure 5)**.

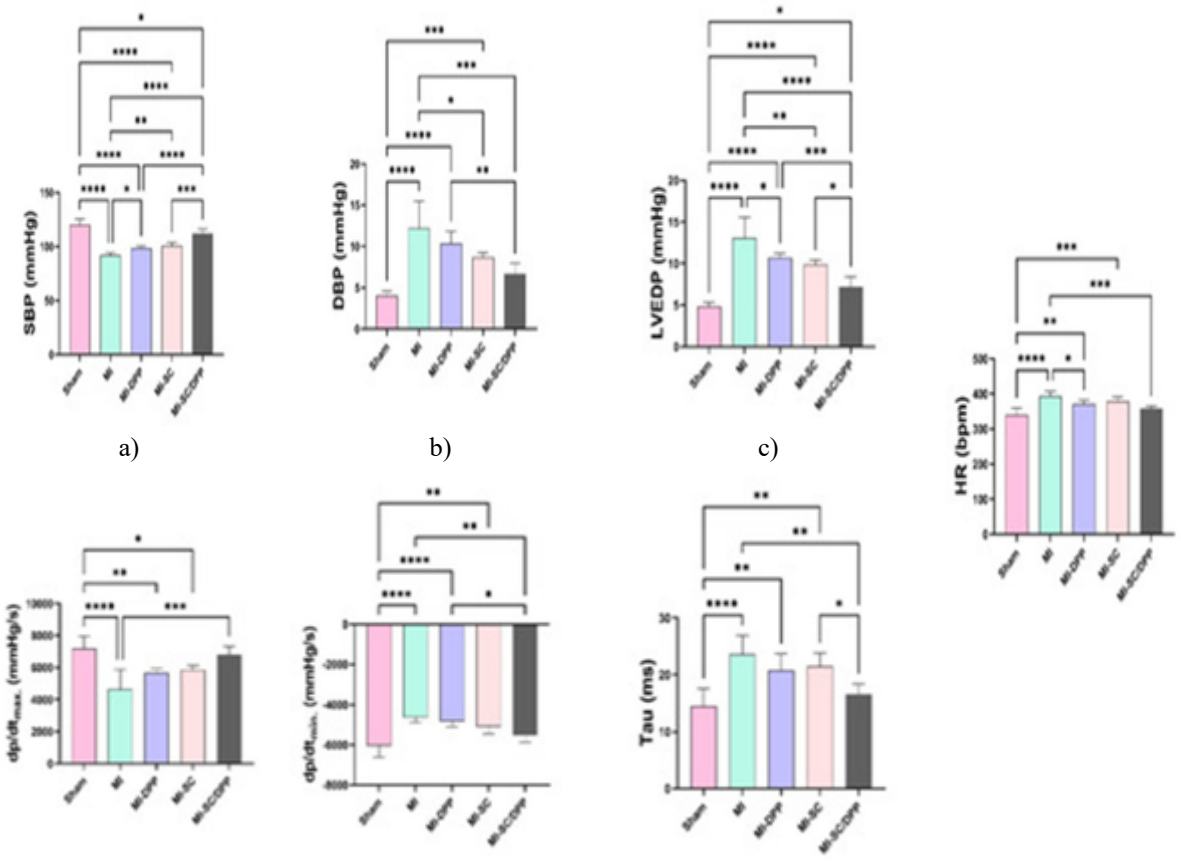

Figure 5. Catheter-based hemodynamic outcomes in all groups following myocardial infarction with or without therapeutic application. Data shown as mean ± SD. *$p < 0.05$, ** $p < 0.01$, *** $p < 0.001$, **** $p < 0.0001$.

Histopathological assessment

Microscopic analyses of cardiac specimens at week 4 (W4) are displayed in **Figures 6 and 7**.

The sham hearts exhibited normal myocardial organization without visible damage. In contrast, MI sections demonstrated heavy inflammatory infiltration, widespread fibrotic deposition, and significant interstitial edema, accompanied by disrupted and misaligned myofibers.

These pathological abnormalities were less severe in all treatment groups, though the degree of recovery varied. Quantitative histology confirmed that treatment notably supported cardiac repair and mitigated ventricular remodeling, as seen in the reduced injury scores: 3.67 ± 0.47, 2.83 ± 0.69, 2.67 ± 0.47, and 1.33 ± 0.47 for MI, MI-DPP, MI-SC, and MI-SC/DPP, respectively.

Scores for MI-SC and MI-SC/DPP were both below those of MI-DPP, with MI-SC/DPP achieving the lowest

value **(Figure 6)**.

Masson's Trichrome (MTC) staining further revealed pronounced fibrosis in the MI group, identified by dense blue collagen fibers. The extent of fibrotic tissue decreased progressively across treated groups, reaching its minimum in MI-SC/DPP. Quantitative fibrosis percentage analysis showed significantly smaller areas in MI-SC/DPP animals (15.83 ± 2.72) compared to MI-SC (28.37 ± 4.22), MI-DPP (31.5 ± 4.01), MI (48.33 ± 7.38), and Sham (0.00 ± 0.00) **(Figure 7)**.

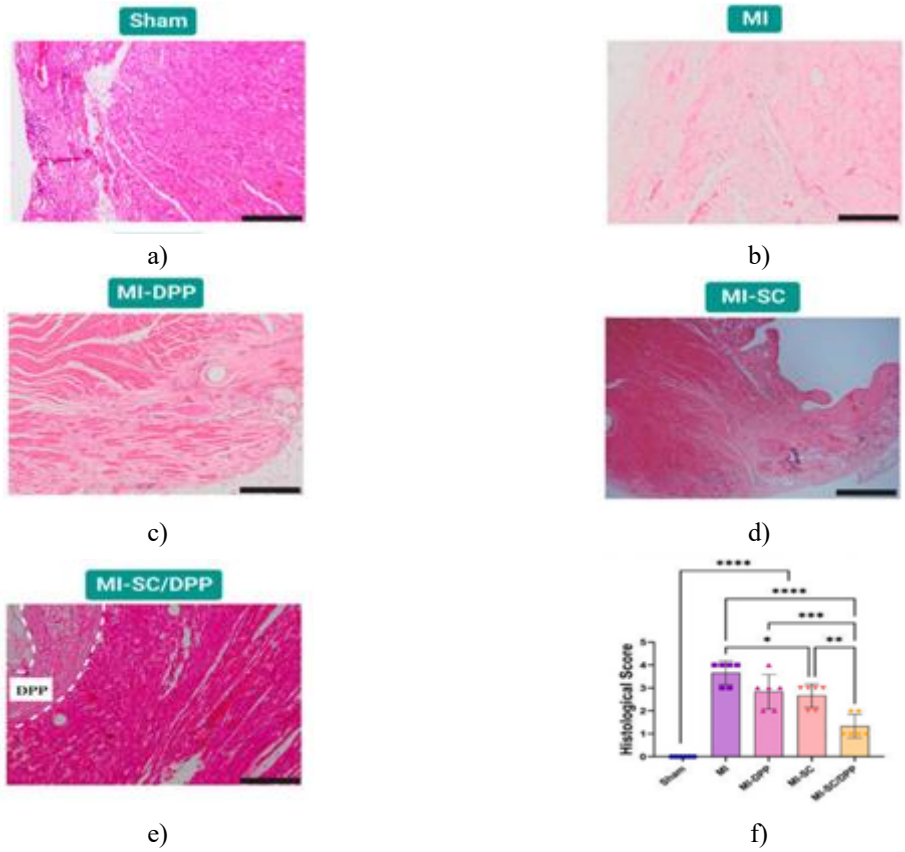

Figure 6. Histological analysis of myocardial tissues stained with Hematoxylin and Eosin (H&E) at four weeks post-MI surgery. Quantitative data presented as mean ± SD.
Scale bar: 200 µm. * $p < 0.05$, ** $p < 0.01$, *** $p < 0.001$, **** $p < 0.0001$.

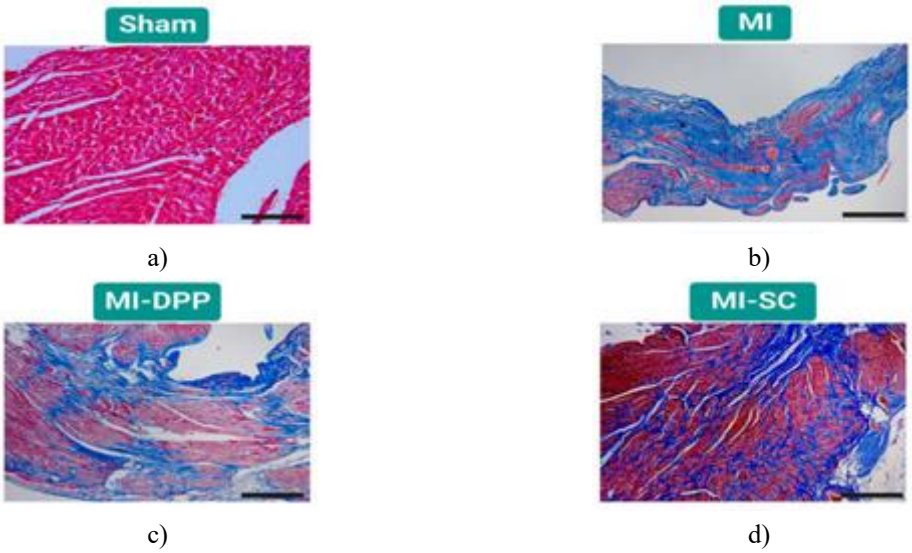

e) f)

Figure 7. Histological analysis of myocardial tissues stained with Hematoxylin and Eosin (H&E) at four weeks post-MI surgery. Quantitative data presented as mean ± SD.
Scale bar: 200 μm. * $p < 0.05$, ** $p < 0.01$, *** $p < 0.001$, **** $p < 0.0001$.

This study was designed to introduce an r-AdMSCs-seeded decellularized porcine pericardium (DPP) construct as a potential therapeutic scaffold for cardiac tissue engineering (CTE). Stem cell therapy has long been considered a valuable approach for patients with ischemic damage or ventricular dysfunction, offering the potential to recover myocardial performance. However, in cases with extensive fibrotic scarring, cell therapy alone has shown limited efficacy due to poor engraftment and low survival rates [21].

When compared with the MI group, both the MI-DPP and MI-SC treatments promoted partial myocardial regeneration, as indicated by improvements in structural echocardiographic indices (LVIDd, LVIDs, IVSd, IVSs, LVPWd, LVPWs, and LVM) and functional markers (EF and FS). Similarly, diastolic performance parameters (E, A, E/A, E/e′, and lateral/septal TDI) displayed notable enhancement relative to the untreated infarcted hearts. These findings are consistent with earlier reports highlighting the regenerative and functional recovery potential of similar interventions [45, 50–52].

Stem cells contribute significantly to angiogenesis through sustained paracrine signaling, though limited retention and engraftment remain persistent issues [45]. Various delivery techniques—such as intravenous infusion [53], intracoronary administration [54], or direct epicardial/endocardial injection [52, 55, 56]—have demonstrated only modest cell survival and homing efficiency [50].

Consequently, the use of decellularized biomaterials, as applied in this study, represents a strategic alternative for cardiac repair. The decellularized extracellular matrix (dECM) retains key structural molecules—collagens, glycosaminoglycans, and proteoglycans—that collectively create a biocompatible microenvironment ideal for cardiomyocyte adhesion, proliferation, and differentiation [16, 57]. When employed as bioactive patches, dECM-based constructs—either alone or in combination with cells, growth factors (GFs), or biopolymers—can significantly promote myocardial regeneration [58].

Previous studies have demonstrated cell infiltration and vascularization within the dECM within 7 days post-implantation [59]. Compared with isolated cell clusters, dECM-embedded cells (e.g., hiPSC-CMs) displayed enhanced electrophysiological activity and maturation, leading to reduced infarct area and higher EF after implantation [60].

In the current experiment, the DPP seeded with stem cells showed greater therapeutic efficacy than either DPP or stem cells used individually, confirming the synergistic effect of combining both components. These results align with prior findings demonstrating improved cardiac repair through dual therapy [21, 43, 45].

Two-dimensional biological scaffolds or cardiac patches serve as efficient cell carriers, enabling enhanced retention at the infarct site while supplying mechanical reinforcement along the ventricular wall [50]. Our r-AdMSC-loaded cardiac patches, when applied to rats with acute MI, significantly improved left ventricular function and remained structurally and functionally stable for at least four weeks. Previous studies have shown that engineered human cardiac patches support long-term cell survival far better than direct myocardial injections, where transplanted cells typically die within weeks [61]. Thus, the improved cardiac recovery observed in our study may be directly linked to prolonged survival and engraftment of the r-AdMSCs delivered via the DPP patch. Supportive evidence from IVPG, hemodynamic, and histological analyses further reinforces this conclusion. Prior studies have linked MA IVPG to myocardial motion and the E wave velocity to basal IVPG [62]. Furthermore, the E/e′ ratio remains a critical diagnostic metric in the grading of diastolic dysfunction, as highlighted by recent LV diastolic function guidelines [63].

To our knowledge, this is the first report to demonstrate the applicability of IVPG, a non-invasive CMME-derived imaging method, for evaluating post-MI cardiac recovery following stem cell–scaffold-based treatment.

Conclusion

In summary, the stem cell–integrated DPP scaffold exhibited a strong synergistic capacity to promote myocardial regeneration and restore cardiac functionality after myocardial infarction, outperforming the individual use of either stem cells or DPP alone. Additionally, the IVPG technique emerged as a precise and innovative diagnostic imaging tool for evaluating functional recovery in post-infarction cardiac tissue.

Acknowledgments: None

Conflict of Interest: None

Financial Support: None

Ethics Statement: None

References

1. World Health Organization. WHO Reveals Leading Causes of Death and Disability Worldwide: 2000–2019. Geneva: WHO;2020.
2. Finegold JA, Asaria P, Francis DP. Mortality from ischaemic heart disease by country, region, and age: Statistics from World Health Organisation and United Nations. Int J Cardiol. 2013;168(2):934–45.
3. Ji ST, Kim H, Yun J, Chung JS, Kwon SM. Promising Therapeutic Strategies for Mesenchymal Stem Cell-Based Cardiovascular Regeneration: From Cell Priming to Tissue Engineering. Stem Cells Int. 2017;2017:3945403.
4. El-Husseiny HM, Mady EA, El-Dakroury WA, Doghish AS, Tanaka R. Stimuli-responsive hydrogels: Smart state of-the-art platforms for cardiac tissue engineering. Front Bioeng Biotechnol. 2023;11:1174075.
5. El-Husseiny HM, Kaneda M, Mady EA, Yoshida T, Doghish AS, Tanaka R. Impact of Adipose Tissue Depot Harvesting Site on the Multilineage Induction Capacity of Male Rat Adipose-Derived Mesenchymal Stem Cells: An In Vitro Study. Int J Mol Sci. 2023;24(14):7513.
6. El-Husseiny HM, Mady EA, Helal MAY, Tanaka R. The Pivotal Role of Stem Cells in Veterinary Regenerative Medicine and Tissue Engineering. Veter Sci. 2022;9(12):648.
7. El-Husseiny HM, Mady EA, Kaneda M, Shimada K, Nakazawa Y, Usui T, et al. Comparison of Bovine- and Porcine-Derived Decellularized Biomaterials: Promising Platforms for Tissue Engineering Applications. Pharmaceutics. 2023;15(6):1906.
8. Ma T, Sun J, Zhao Z, Lei W, Chen Y, Wang X, et al. A brief review: Adipose-derived stem cells and their therapeutic potential in cardiovascular diseases. Stem Cell Res Ther. 2017;8(1):124.
9. Houtgraaf JH, Dekker WKD, van Dalen BM, Springeling T, de Jong R, van Geuns RJ, et al. First Experience in Humans Using Adipose Tissue–Derived Regenerative Cells in the Treatment of Patients With ST-Segment Elevation Myocardial Infarction. J Am Coll Cardiol. 2012;59(6):539–40.
10. Penn MS, Mangi AA. Genetic Enhancement of Stem Cell Engraftment, Survival, and Efficacy. Circ Res. 2008;102(12):1471–82.
11. Kanda M, Nagai T, Kondo N, Matsuura K, Akazawa H, Komuro I, et al. Pericardial Grafting of Cardiac Progenitor Cells in Self-Assembling Peptide Scaffold Improves Cardiac Function After Myocardial Infarction. Cell Transplant. 2023;32:09636897231174078.
12. Tanaka T, Hara S, Hendawy H, El-Husseiny HM, Tanaka R, Asakura T. Development of Small-Diameter Artificial Vascular Grafts Using Transgenic Silk Fibroin. Prosthesis. 2023;5(4):763–73.
13. Texakalidis P, Giannopoulos S, Charisis N, Giannopoulos S, Karasavvidis T, Koullias G, et al. A meta-analysis of randomized trials comparing bovine pericardium and other patch materials for carotid endarterectomy. J Vasc Surg. 2018;68(4):1241–56.e1.
14. Kameli SM, Khorramirouz R, Eftekharzadeh S, Fendereski K, Daryabari SS, Tavangar SM, et al. Application of tissue-engineered pericardial patch in rat models of myocardial infarction. J Biomed Mater Res A. 2018;106(10):2670–8.

15. Kajbafzadeh AM, Tafti SHA, Khorramirouz R, Sabetkish S, Kameli SM, Orangian S, et al. Evaluating the role of autologous mesenchymal stem cell seeded on decellularized pericardium in the treatment of myocardial infarction: An animal study. Cell Tissue Bank. 2017;18(3):527–38.
16. Zhu D, Li Z, Huang K, Caranasos TG, Rossi JS, Cheng K. Minimally invasive delivery of therapeutic agents by hydrogel injection into the pericardial cavity for cardiac repair. Nat Commun. 2021;12(1):1412.
17. Li M, Wu H, Yuan Y, Hu B, Gu N. Recent fabrications and applications of cardiac patch in myocardial infarction treatment. View. 2022;3(1):20200153.
18. Yao Y, Li A, Wang S, Lu Y, Xie J, Zhang H, Zhang D, et al. Multifunctional elastomer cardiac patches for preventing left ventricle remodeling after myocardial infarction in vivo. Biomaterials. 2022;282:121382.
19. Zhang X, Sun Y, Wu T, Zhao X, Yang R, Wang H, Liu W. Combined intramyocardial injectable hydrogel and pericardial adhesive hydrogel patch therapy strategy to achieve gene/ion/gas delivery for improving cardiac function. Nano Today. 2023;50:101861.
20. Meyer T, Cebotari S, Brandes G, Hartung D, Wacker F, Theis M, et al. Decellularized Porcine Pericardium Enhances Autologous Vascularized Matrix as a Prosthesis for Left Ventricular Full-Wall Myocardial Reconstruction. Prosthesis. 2023;5(1):113–29.
21. Hashizume R, Fujimoto KL, Hong Y, Guan J, Toma C, Tobita K, et al. Biodegradable elastic patch plasty ameliorates left ventricular adverse remodeling after ischemia–reperfusion injury: A preclinical study of a porous polyurethane material in a porcine model. J Thorac Cardiovasc Surg. 2013;146(2):391–9.e1.
22. Wei HJ, Chen SC, Chang Y, Hwang SM, Lin WW, Lai PH, et al. Porous acellular bovine pericardia seeded with mesenchymal stem cells as a patch to repair a myocardial defect in a syngeneic rat model. Biomaterials. 2006;27(24):5409–19.
23. El-Husseiny H. Evaluation of Some Prosthetic Implants for Surgical Management of Different Varieties of Hernias in Domestic Animals. Banha, Egypt: Faculty of Veterinary Medicine, Benha University;2017. p. 42–3.
24. El-Husseiny MH. Platelet Rich Fibrin Augmented Versus Non-Augmented Glycerolized Bovine Pericardium and Polypropylene Mesh for Repairing of Large Abdominal Wall Defects. Eur J Med Nat Sci. 2020;3(2):33–48.
25. Badylak SF, Kochupura PV, Cohen IS, Doronin SV, Saltman AE, Gilbert TW, et al. The Use of Extracellular Matrix as an Inductive Scaffold for the Partial Replacement of Functional Myocardium. Cell Transplant. 2006;15(1):29–40.
26. Ruel MA, Sellke FW, Bianchi C, Khan TA, Faro R, Zhang JP, Cohn WE. Endogenous myocardial angiogenesis and revascularization using a gastric submucosal patch. Ann Thorac Surg. 2003;75(5):1443–9.
27. Tudorache I, Kostin S, Meyer T, Teebken O, Bara C, Hilfiker A, et al. Viable vascularized autologous patch for transmural myocardial reconstruction. Eur J Cardiothorac Surg. 2009;36(2):306–11.
28. Nazari H, Heirani-Tabasi A, Esmaeili E, Kajbafzadeh AM, Hassannejad Z, Boroomand S, et al. Decellularized human amniotic membrane reinforced by MoS2-Polycaprolactone nanofibers, a novel conductive scaffold for cardiac tissue engineering. J Biomater Appl. 2022;36(11):1527–39.
29. Rane AA, Christman KL. Biomaterials for the Treatment of Myocardial Infarction. J Am Coll Cardiol. 2011;58(26):2615–29.
30. Zhou Q, Zhou JY, Zheng Z, Zhang H, Hu SS. A novel vascularized patch enhances cell survival and modifies ventricular remodeling in a rat myocardial infarction model. J Thorac Cardiovasc Surg. 2010;140(6):1388–96.e3.
31. Araña M, Gavira JJ, Peña E, González A, Abizanda G, Cilla M, et al. Epicardial delivery of collagen patches with adipose-derived stem cells in rat and minipig models of chronic myocardial infarction. Biomaterials. 2014;35(1):143–51.
32. Crapo PM, Gilbert TW, Badylak SF. An overview of tissue and whole organ decellularization processes. Biomaterials. 2011;32(12):3233–43.
33. Schmidt CE, Baier JM. Acellular vascular tissues: Natural biomaterials for tissue repair and tissue engineering. Biomaterials. 2000;21(22):2215–31.
34. Hennessy RS, Go JL, Hennessy RR, Tefft BJ, Jana S, Stoyles NJ, et al. Recellularization of a novel off-the-shelf valve following xenogenic implantation into the right ventricular outflow tract. PLoS ONE. 2017;12(6):e0181614.

35. Khorramirouz R, Go JL, Noble C, Morse D, Lerman A, Young MD. In Vivo Response of Acellular Porcine Pericardial for Tissue Engineered Transcatheter Aortic Valves. Sci Rep. 2019;9(1):1094.
36. Schu S, Nosov M, O'Flynn L, Shaw G, Treacy O, Barry F, Murphy M, et al. Immunogenicity of allogeneic mesenchymal stem cells. J Cell Mol Med. 2012;16(9):2094–103.
37. Hou D, Youssef EA-S, Brinton TJ, Zhang P, Rogers P, Price ET, et al. Radiolabeled cell distribution after intramyocardial, intracoronary, and interstitial retrograde coronary venous delivery: Implications for current clinical trials. Circulation. 2005;112(19 Suppl):I150–6.
38. Teng CJ, Luo J, Chiu RC, Shum-Tim D. Massive mechanical loss of microspheres with direct intramyocardial injection in the beating heart: Implications for cellular cardiomyoplasty. J Thorac Cardiovasc Surg. 2006;132(3):628–32.
39. Ciampi Q, Villari B. Role of echocardiography in diagnosis and risk stratification in heart failure with left ventricular systolic dysfunction. Cardiovasc Ultrasound. 2007;5(1):34.
40. El-Husseiny HM, Mady EA, Takahashi K, Tanaka R. Intraventricular pressure gradient: A novel colour M-mode echocardiographic-derived imaging modality to assess and predict the alterations following acute myocardial infarction. Eur Heart J. 2023;44(40):ehac779-004.
41. El-Husseiny HM. In Vitro and In Vivo Evaluation of Stem Cell-Seeded Biomaterials for Cardiac Tissue Engineering after Myocardial Infarction. Fuchu, Japan: Tokyo University of Agriculture and Technology; 2023.
42. Ramm R, Goecke T, Theodoridis K, Hoeffler K, Sarikouch S, Findeisen K, et al. Decellularization combined with enzymatic removal of N-linked glycans and residual DNA reduces inflammatory response and improves performance of porcine xenogeneic pulmonary heart valves in an ovine in vivo model. Xenotransplantation. 2020;27(5):e12571.
43. Tan MY, Zhi W, Wei RQ, Huang YC, Zhou KP, Tan B, et al. Repair of infarcted myocardium using mesenchymal stem cell seeded small intestinal submucosa in rabbits. Biomaterials. 2009;30(17):3234–40.
44. Sharma NM, Cunningham CJ, Zheng H, Liu X, Patel KP. Hypoxia-Inducible Factor-1α Mediates Increased Sympathoexcitation via Glutamatergic N-Methyl-d-Aspartate Receptors in the Paraventricular Nucleus of Rats with Chronic Heart Failure. Circ Heart Fail. 2016;9(7):e003423.
45. Park SJ, Kim RY, Park BW, Lee S, Choi SW, Park JH, et al. Dual stem cell therapy synergistically improves cardiac function and vascular regeneration following myocardial infarction. Nat Commun. 2019;10(1):3123.
46. Kim H, Park SJ, Park JH, Lee S, Park BW, Lee SM, et al. Enhancement strategy for effective vascular regeneration following myocardial infarction through a dual stem cell approach. Exp Mol Med. 2022;54(8):1165–78.
47. Rychik J, Ayres N, Cuneo B, Gotteiner N, Hornberger L, Spevak PJ, et al. American society of echocardiography guidelines and standards for performance of the fetal echocardiogram. J Am Soc Echocardiogr. 2004;17(8):803–10.
48. Zacchigna S, Paldino A, Falcão-Pires I, Daskalopoulos EP, Ferro MD, Vodret S, et al. Towards standardization of echocardiography for the evaluation of left ventricular function in adult rodents: A position paper of the ESC Working Group on Myocardial Function. Cardiovasc Res. 2021;117(1):43–59.
49. Shi K, Zhao W, Chen Y, Ho WT, Yang P, Zhao ZJ. Cardiac hypertrophy associated with myeloproliferative neoplasms in JAK2V617F transgenic mice. J Hematol Oncol. 2014;7(1):25.
50. Carvalho E, Verma P, Hourigan K, Banerjee R. Myocardial infarction: Stem cell transplantation for cardiac regeneration. Regen Med. 2015;10(8):1025–43.
51. Choi YS, Dusting GJ, Stubbs S, Arunothayaraj S, Han XL, Collas P, et al. Differentiation of human adipose-derived stem cells into beating cardiomyocytes. J Cell Mol Med. 2010;14(4):878–89.
52. Gyöngyösi M, Lang I, Dettke M, Beran G, Graf S, Sochor H, et al. Combined delivery approach of bone marrow mononuclear stem cells early and late after myocardial infarction: The MYSTAR prospective, randomized study. Nat Clin Pract Cardiovasc Med. 2009;6(2):70–81.
53. Barbash IM, Chouraqui P, Baron J, Feinberg MS, Etzion S, Tessone A, et al. Systemic Delivery of Bone Marrow–Derived Mesenchymal Stem Cells to the Infarcted Myocardium. Circulation. 2003;108(7):863–8.
54. Janssens S, Dubois C, Bogaert J, Theunissen K, Deroose C, Desmet W, et al. Autologous bone marrow-derived stem-cell transfer in patients with ST-segment elevation myocardial infarction: Double-blind, randomised controlled trial. Lancet. 2006;367(9515):113–21.

55. Perin EC, López J. Methods of stem cell delivery in cardiac diseases. Nat Clin Pract Cardiovasc Med. 2006;3(Suppl 1):S110–3.
56. Sherman W, Martens TP, Viles-Gonzalez JF, Siminiak T. Catheter-based delivery of cells to the heart. Nat Clin Pract Cardiovasc Med. 2006;3(Suppl 1):S57–64.
57. Xing H, Lee H, Luo L, Kyriakides TR. Extracellular matrix-derived biomaterials in engineering cell function. Biotechnol Adv. 2020;42:107421.
58. Sarig U, Sarig H, De-Berardinis E, Chaw SY, Nguyen EB, Ramanujam VS, et al. Natural myocardial ECM patch drives cardiac progenitor based restoration even after scarring. Acta Biomater. 2016;44:209–20.
59. Shah M, Kc P, Zhang G. In Vivo Assessment of Decellularized Porcine Myocardial Slice as an Acellular Cardiac Patch. ACS Appl Mater Interfaces. 2019;11(26):23893–900.
60. Wang Q, Yang H, Bai A, Jiang W, Li X, Wang X, et al. Functional engineered human cardiac patches prepared from nature's platform improve heart function after acute myocardial infarction. Biomaterials. 2016;105:52–65.
61. Passier R, van Laake LW, Mummery CL. Stem-cell-based therapy and lessons from the heart. Nature. 2008;453(7193):322–9.
62. Iwano H, Kamimura D, Fox E, Hall M, Vlachos P, Little WC. Altered Spatial Distribution of the Diastolic Left Ventricular Pressure Difference in Heart Failure. J Am Soc Echocardiogr. 2015;28(6):597–605.e1.
63. Nagueh SF, Smiseth OA, Appleton CP, Byrd BF 3rd, Dokainish H, Edvardsen T, et al. Recommendations for the Evaluation of Left Ventricular Diastolic Function by Echocardiography: An Update from the American Society of Echocardiography and the European Association of Cardiovascular Imaging. Eur Heart J Cardiovasc Imaging. 2016;17(12):1321–60.